July 31, 2009

Surface Geometry of C60 on Ag(111)

H. I. Li, *Pennsylvania State University*
K. Pussi, *Lappeenranta University of Technology*
K. J. Hanna, *Pennsylvania State University*
Lin-Lin Wang, *University of Illinois at Urbana-Champaign*
Duane D. Johnson, *University of Illinois at Urbana-Champaign*, et al.

Surface Geometry of C_{60} on Ag(111)

H. I. Li,[1] K. Pussi,[2] K. J. Hanna,[1] L.-L. Wang,[3] D. D. Johnson,[3] H.-P. Cheng,[4] H. Shin,[1] S. Curtarolo,[5] W. Moritz,[6] J. A. Smerdon,[7] R. McGrath,[7] and R. D. Diehl[1]

[1]*Department of Physics, The Pennsylvania State University, University Park, Pennsylvania 16802, USA*
[2]*Department of Mathematics and Physics, Lappeenranta University of Technology, Lappeenranta, Finland*
[3]*Department of Materials Science and Engineering, University of Illinois at Urbana-Champaign, Urbana, Illinois 61801, USA*
[4]*Quantum Theory Project and Department of Physics, University of Florida, Gainesville, Florida 32611, USA*
[5]*Department of Mechanical Engineering and Materials Science, Duke University, Durham, North Carolina 27708, USA*
[6]*Department of Earth & Environmental Science, University of Munich, D-80333 Munich, Germany*
[7]*Surface Science Research Centre, University of Liverpool, Liverpool, L69 3BX, United Kingdom*

(Received 16 April 2009; published 27 July 2009)

The geometry of adsorbed C_{60} influences its collective properties. We report the first dynamical low-energy electron diffraction study to determine the geometry of a C_{60} monolayer, Ag(111)-$(2\sqrt{3} \times 2\sqrt{3})30°$-$C_{60}$, and related density functional theory calculations. The stable monolayer has C_{60} molecules in vacancies that result from the displacement of surface atoms. C_{60} bonds with hexagons down, with their mirror planes parallel to that of the substrate. The results indicate that vacancy structures are the rule rather than the exception for C_{60} monolayers on close-packed metal surfaces.

DOI: 10.1103/PhysRevLett.103.056101 PACS numbers: 68.43.Fg, 61.05.jh, 61.48.−c, 68.35.bp

Fullerene-based molecular crystals and films are of interest because of their very rich electronic properties, including superconductivity with high critical temperatures, ferromagnetism, and metal-insulator transitions [1]. The interfaces of C_{60} films with metal surfaces are of particular interest for molecular electronics [2]. C_{60} films are also of interest from a fundamental perspective, because they represent a class of relatively simple model structures for studying the interactions of gases with carbon materials [3]. Although the variety of phenomena observed in C_{60} films is exceptional, the C_{60}-substrate interaction is far from being understood. While the C_{60} geometry is critical to the properties of the films [4,5], an unequivocal determination of the C_{60} adsorption geometry has been elusive [6].

Two STM studies of C_{60} on Ag(111) at room temperature (RT) found that the monolayer has a commensurate $(2\sqrt{3} \times 2\sqrt{3})R30°$ structure (nearest-neighbor distance 10.01 Å), that consists of a mixture of two orientations of C_{60} [7–11]. While one of these studies concluded from images of occupied and unoccupied states that one orientation of C_{60} adsorbs in top sites with their pentagonal faces down [7,8], the other concluded that those C_{60} adsorb in hollow sites with their hexagonal faces down [10,12]. An x-ray photoelectron diffraction (XPD) study at RT also concluded that the monolayer is a mixture of two species, one with the C_{60} hexagonal face down, and the other with a C-C bond down [13]. An *ab initio* density functional theory (DFT) calculation for the same structure found that the ground state adsorption geometry is the hcp hollow site, with the hexagonal face down [14]. This mixture of conflicting results, and similar ones for C_{60} on other substrates [6], illustrates the difficulty in establishing the correct adsorption structures for these films.

Diffraction is an ideal method for the determination of the geometries for adsorbed C_{60}. Although low-energy electron diffraction (LEED) is the most common technique for determining surface geometries, it has not yet been applied to a C_{60} film. The computational limitation of LEED has diminished in recent years due to the increase in computing power and the efficiency of LEED codes [15,16]. Now the limiting factor for complex structures is often the size of the experimental data set. For molecular adsorbates, the quantity and quality of the data can be limited due to the Debye-Waller effect from molecular motions. The data presented here were acquired at low T (32 K) in order to damp the molecular motions and maximize the energy range of the LEED data.

The Ag(111) crystal preparation and the C_{60} source were described earlier [17]. The sample was typically dosed at RT to several layers and then heated to desorb all except one monolayer. Although higher layer desorption only requires heating to about 575 K [11], annealing to 685 K produced the best quality LEED patterns. It was reported in an STM study that annealing converts metastable epitaxially rotated phases to the $(2\sqrt{3} \times 2\sqrt{3})R30°$ structure, also observed here [11,12]. Desorption from the monolayer occurs above 685 K. The sample was cooled to 32 K for the LEED measurements [17]. Examples of LEED patterns at several energies are shown in Fig. 1. These patterns exhibit threefold symmetry with one mirror plane. The $I(E)$ curves were extracted for each diffraction spot and the intensities of the symmetrically equivalent spots were averaged, resulting in a data set having an energy length of 4860 eV, a total of 15 beams having a maximum range of 100 to 600 eV.

The LEED calculations used the SATLEED [18] and LEEDFIT [19] codes. The agreement between the experi-

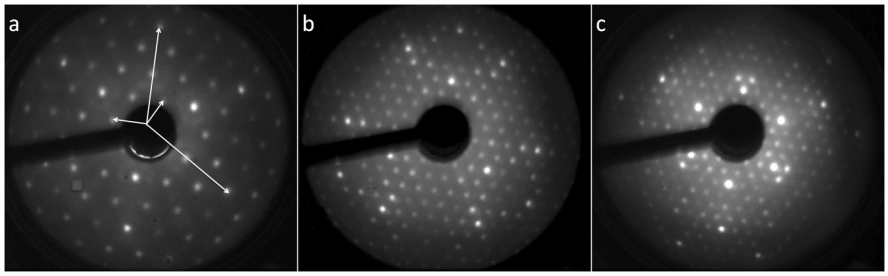

FIG. 1. LEED patterns from Ag(111)-$(2\sqrt{3} \times 2\sqrt{3})R30°$ for incident beam energies of (a) 101 eV, (b) 365 eV, and (c) 504 eV, for a sample T of 32 K. Reciprocal unit cells for the substrate (long arrows) and overlayer (short arrows) are indicated in (a).

ment and calculation was measured using the Pendry R factors, and the statistical errors were calculated using the Pendry RR-function [20]. The crystal potential was calculated from a superposition of atomic potentials for the actual adsorption geometry using optimized muffin tin radii [21]. This resulted in 12 sets of scattering phase shifts from symmetry inequivalent C atoms and 2 for the Ag atoms (one for the surface atoms, one for deeper layers). Only small differences were found compared to calculations using only one set of phase shifts each for C and Ag. The sites tested were top, hcp hollow, fcc hollow, bridge and several types of vacancy sites that correspond to missing (displaced) Ag surface atoms. The tested molecular orientations were hexagon down, pentagon down, and C-C bond down, for different in-plane rotational alignments. Domain averaging was used to achieve the observed symmetry, and mixtures (coherent and incoherent) of sites and C_{60} orientations were also tested.

The time for the calculations ranged from 1 h to several days on a supercluster, depending on the degree of symmetry in the structure. In the first step, two structures gave significantly better R factors: C_{60} on a top site or a vacancy site with its hexagonal face down and with the mirror plane of C_{60} aligned with the mirror plane of Ag(111). This step ruled out all sites except top and vacancy, and all molecular orientations aside from hexagon down with the mirror plane parallel [22]. In the next step, the top and vacancy site structures were relaxed (C_{60} + 5 layers of Ag) according to the symmetry, and then the nonstructural parameters (Debye T and inner potential) were optimized. This resulted in a significantly better fit for the vacancy site structure ($R = 0.36$) compared to the top site structure ($R = 0.42$). The best-fit structure is shown in Fig. 2, with parameters given in Table I. The calculation was not very sensitive to the difference between 0° vs 180° orientation of the molecules.

Aside from the vacancy reconstruction, there is very little displacement of the Ag atoms from their bulk positions. The Ag maintains a layer spacing very close to the bulk, and there is a slight depression of the Ag atoms nearest to the C_{60}. There is also very little relaxation within the C_{60} molecules. The bottom hexagon of the C_{60} has the same diameter as the gas-phase molecule [23]. The bond lengths within the molecule after relaxation range from 1.35 to 1.51 Å, compared to the two bond lengths of 1.40 and 1.46 Å in the gas phase, with no net molecular size change. In light of the DFT study for this surface (below), we also tested vacancy structures with one Ag adatom per unit cell. The agreement was slightly worse, but the existence of an additional Ag atom cannot be ruled out because its effect on the spectra is very small.

Previous studies did not identify a surface reconstruction for this surface. An earlier DFT study indicated that the hollow sites are more stable than the top [14]. We now return to the DFT [24,25] calculations, which in the local density approximation (LDA) [26,27] have been shown to be able to describe both the electronic and energetic properties of adsorbed C_{60} monolayer on metal surfaces

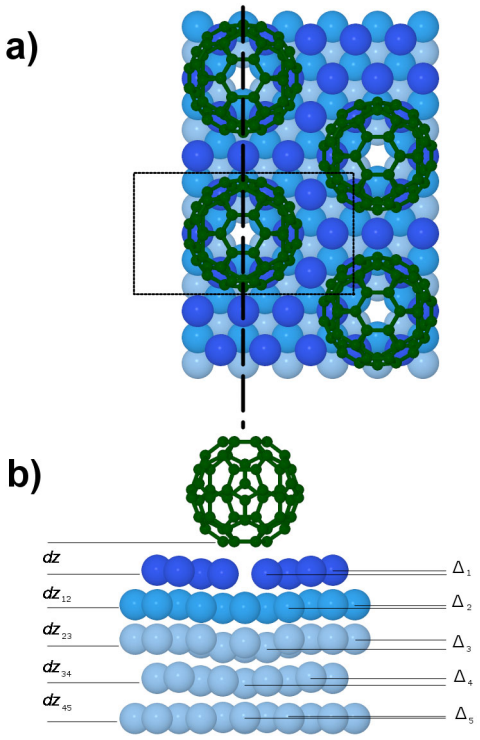

FIG. 2 (color online). (a) Vacancy site structure, showing three layers of Ag. The mirror plane of the molecule is parallel to the mirror plane of the substrate (dashed line). There are two such parallel orientations of the molecules, one as shown, and one rotated 180°. The top hexagon is surrounded by 3 hexagons and 3 pentagons—180° rotation interchanges these (as well as some others that are not visible). (b) Side view of the vacancy structure, viewed from the bottom of (a), along the dashed line, including the atoms in the box on (a). The structural parameters are given in Table I; the buckling is magnified and the atoms are shown with a reduced size for clarity.

TABLE I. Structural parameters for the relaxed C_{60}/Ag(111) in various sites in the $(2\sqrt{3} \times 2\sqrt{3})R30°$ unit cell. dz's correspond to average perpendicular distances, d refers to the average bond distance, Δ's refer to average intralayer buckling amplitude. The numerical subscripts refer to the substrate layers. In the LEED analysis, additional fitted parameters were the Debye T's of the C_{60} film (220 K), the surface Ag (355 K) and the bulk Ag (315 K). The bulk Ag(111) interlayer spacing is 2.35 Å.

(Å)	LEED vacancy	DFT top	DFT vac	DFT hcp
dz (Ag-C_{60})	2.0 ± 0.1	2.29	1.88	2.36
d (Ag-C)	2.5 ± 0.1	2.65	2.35	2.44
dz_{12}	2.36 ± 0.03	2.32	2.29	2.31
dz_{23}	2.33 ± 0.04	2.32	2.32	2.32
dz_{34}	2.34 ± 0.06	2.33	2.32	2.33
dz_{45}	2.34 ± 0.1	2.33	2.32	2.33
Δ_1	0.02 ± 0.03	0.29	0.04	0.06
Δ_2	0.03 ± 0.04	0.07	0.04	0.10
Δ_3	0.03 ± 0.05	0.04	0.01	0.01
Δ_4	0.02 ± 0.07	0.02	0.01	0.00
Δ_5	0.01 ± 0.2	...	...	...

[14,28–30]. The setup of the slab calculation can be found elsewhere [14]. Here, we considered additional structures having substrate reconstructions. One is the vacancy (vac) structure, where the Ag atom beneath the C_{60} in the top structure is removed, and the other is the reconstructed (rec) structure, where the dispatched Ag atom is put back onto the Ag surface as an adatom in an interstitial site among neighboring C_{60}'s.

In Table II, the calculated adsorption energies of different structures are listed. The structural parameters after relaxation for the vac structure are listed in Table I. For all the different sites, we find that the preferred orientation of C_{60} is with a hexagon facing down and its vertical mirror plane along the substrate mirror plane. The top site is the least favorable; it includes a 0.29 Å inward relaxation of the Ag atom beneath C_{60}, which costs considerable elastic energy.

For comparison, we have listed in Table II the calculated adsorption energies for C_{60}/Au(111), and for C_{60}/Al(111) from Ref. [28], where a vacancy-adatom mechanism was proposed to explain the structural transition observed in STM [32]. Similarly, we find that C_{60} binds much more strongly to the vacancy site on Au(111), indicated by the large increase of adsorption energy in the vac structure. To include the vacancy formation energy, we put the dispatched Ag atom back onto the surface and used the unreconstructed Ag(111) surface as an energy reference. After further relaxation, the Ag adatom finds an equilibrium position slightly off the fcc site between two C_{60}'s. The adsorption energy of this rec structure is still larger than the unreconstructed hcp structure by 0.07 eV, which indeed shows that the vacancy site is the preferred one in the $(2\sqrt{3} \times 2\sqrt{3})R30°$ structure.

TABLE II. Ag(111), Al(111), and Au(111) vacancy formation energy (E_{vac}) and adsorption energies (E_{ads}) of C_{60} on the different sites in the $(2\sqrt{3} \times 2\sqrt{3})R30°$ unit cell. For C_{60}/Al(111), E_{ads} are from Ref. [28] and E_{vac} is from Ref. [31], where the $(\sqrt{3} \times \sqrt{3})R30°$ unit cell was used.

	E_{vac} (eV)	E_{ads} (eV)			
		top	hcp	rec	vac
C_{60}/Ag(111)	0.67	1.27	1.52	1.59	2.61
C_{60}/Al(111)	0.36	0.98	1.37	1.40	2.34
C_{60}/Au(111)	0.83	0.86	1.25	1.35	2.69

Insight about the vacancy-adatom mechanism is gained by comparing C_{60}/Ag(111) with C_{60}/Al(111) as listed in Table II. Although the vacancy creation cost on Ag(111) is larger, the adsorption energies for C_{60}/Ag(111) are always bigger than C_{60}/Al(111), and are comparable to the difference in the vacancy formation energies. Hence, the stronger C_{60}-Ag interaction can compensate that energy difference, and the reconstruction becomes viable. A vacancy structure also has been observed in a recent surface x-ray diffraction experiment on C_{60}/Pt(111) [33]. In that case, the much stronger C_{60}-Pt interaction can cause a Pt(111) reconstruction [33], even though the vacancy formation energy for Pt is much larger. Compared to Ag, Pt has a d band much closer to the Fermi level, which facilitates stronger band hybridization and more covalent bonding with C_{60}, and thus larger binding energy.

With hindsight, the earlier STM studies provided some evidence for a surface reconstruction. For adsorption at RT, several different phases were observed, one of them corresponding to a $(2\sqrt{3} \times 2\sqrt{3})R30°$ structure, the others corresponding to several metastable incommensurate or higher-order commensurate structures with lattice rotations, which convert into the $(2\sqrt{3} \times 2\sqrt{3})R30°$ structure upon annealing [11]. Before annealing, the molecules in all structures have the same intensities in the STM images. Upon annealing to 573 K, however, the appearance of the molecules in the $(2\sqrt{3} \times 2\sqrt{3})R30°$ structure changes, and they are imaged as "bright" and "dim" in the STM. Sufficient annealing converts the epitaxially rotated phases entirely to this "mixed" $(2\sqrt{3} \times 2\sqrt{3})R30°$ phase [7,8,10–12]. The bright and dim molecules were attributed to different orientations of the molecules, and were observed to "flip" from one to the other during experiments at RT [11]. The mixture of bright and dim molecules may correspond to the mixture of orientations observed with XPD at RT [13]. We propose that the uniform-intensity molecules imaged after deposition at RT but before annealing, correspond to molecules that are on the surface, possibly rotating. Heating produces the vacancy structure, which has two orientations of C_{60}'s that image differently. This is consistent with the earlier STM study that found that the $(2\sqrt{3} \times 2\sqrt{3})R30°$ structure is more stable after annealing the overlayer [11], and the with XPD study that found two orientations in the annealed monolayer [13].

As stated before, the LEED pattern improves markedly after annealing to 685 K; i.e., the diffraction spots sharpen

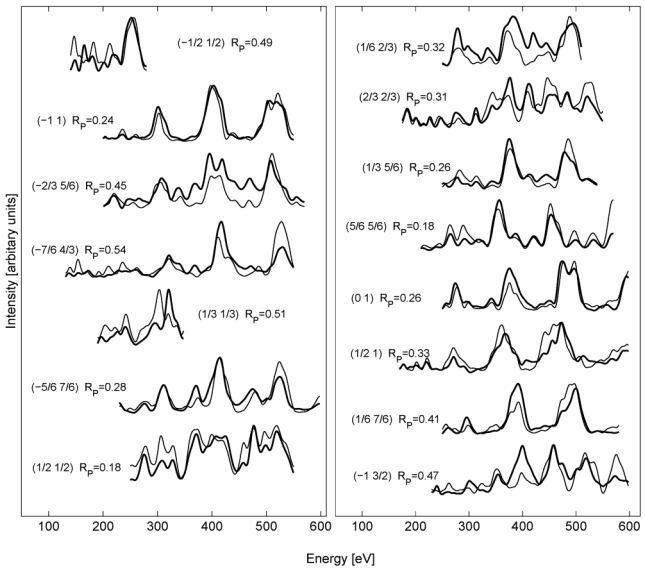

FIG. 3. Experimental (bold line) and best-fit calculated spectra for the Ag(111)-$(2\sqrt{3} \times 2\sqrt{3})R30°$ structure. Individual beam R factors are given. The overall R factor is 0.36.

and the background diminishes. The primary reason for this improvement is likely the reduction in domain boundaries as the epitaxially rotated regions convert to the $(2\sqrt{3} \times 2\sqrt{3})R30°$ structure. Even after annealing, however, there is a considerable Debye-Waller factor at 300 K, suggesting considerable dynamical disorder, such as molecular rotations or librations, consistent with the STM observation of flipping at RT. From the LEED analysis at 32 K, there is no evidence for other orientations, suggesting that while such molecules that may exist at RT [13], they adopt the lower-energy hexagon-down orientation at low T. The experimental and calculated spectra are shown in Fig. 3. Since annealing to at least 573 K is the most common method for producing a monolayer of C_{60} on Ag(111), most experiments that have been performed on this surface are likely for C_{60} in vacancy sites [4,7,8,10–13,30,34–36].

We have demonstrated that a monolayer of C_{60} on Ag(111) induces a substrate reconstruction, producing vacancies that are occupied by C_{60}. This phenomenon is related to the relative energies of vacancy formation and chemisorption. Our DFT calculations show that on both Ag(111) and Au(111), the balance favors reconstruction. A previous DFT study indicated the same for C_{60} on Al(111) [28]. Until now, although reconstructions were often observed for C_{60} adsorption on other surfaces, they were thought to be uncommon for C_{60} adsorption on close-packed noble metal substrates, where the bonding is regarded as mainly ionic, even though reconstructions were reported for C_{60} on Cu(111) [37]. This study demonstrates the utility of LEED for the determination of large molecule adsorption geometries. In light of these results, it seems probable that the observed preference for C_{60} adsorption along the zigzag steps [38] may also involve vacancy reconstructions.

We acknowledge useful communications with Y.-M. Byun and L. W. Bruch, experimental assistance from J. Stevens, and support from NSF grants DMR-0505160, DMR-03-25939, and DMR-0639822, Academy of Finland Project No. 204726, US/DOE/DEFG02-03ER15476, US/DOE/DEFG02-03ER46026, and US/DOE/DEFG02-02ER45995.

[1] E. Osawa, *Perspectives in Fullerene Nanotechnology* (Kluwer Academic Publishers, Dordrecht, 2002).
[2] M. C. Petty, *Molecular Electronics* (Wiley-Interscience, Chichester, 2007).
[3] S. M. Gatica *et al.*, J. Low Temp. Phys. **152**, 89 (2008).
[4] V. Brouet *et al.*, Phys. Rev. Lett. **93**, 197601 (2004).
[5] V. Brouet *et al.*, Phys. Rev. Lett. **95**, 099903(E) (2005).
[6] J. A. Larsson *et al.*, Phys. Rev. B **77**, 115434 (2008).
[7] E. I. Altman and R. J. Colton, Phys. Rev. B **48**, 18 244 (1993).
[8] E. I. Altman and R. J. Colton, Surf. Sci. **295**, 13 (1993).
[9] T. Hashizume and T. Sakurai, Surf. Rev. Lett. **3**, 905 (1996).
[10] T. Sakurai *et al.*, Appl. Surf. Sci. **87–88**, 405 (1995).
[11] X. D. Wang *et al.*, Scanning Microsc. **8**, 987 (1994).
[12] T. Sakurai *et al.*, Prog. Surf. Sci. **51**, 263 (1996).
[13] A. Tamai *et al.*, Phys. Rev. B **72**, 085421 (2005).
[14] L. L. Wang and H. P. Cheng, Phys. Rev. B **69**, 165417 (2004).
[15] G. M. Gavaza *et al.*, Phys. Rev. Lett. **97**, 055505 (2006).
[16] G. M. Gavaza *et al.*, J. Phys. Condens. Matter **20**, 304202 (2008).
[17] S. M. Gatica *et al.*, Phys. Rev. B **77**, 045414 (2008).
[18] M. A. Van Hove *et al.*, Surf. Sci. Rep. **19**, 191 (1993).
[19] H. Over *et al.*, Phys. Rev. B **46**, 15 438 (1992).
[20] J. B. Pendry, J. Phys. C **13**, 937 (1980).
[21] J. Rundgren, Phys. Rev. B **68**, 125405 (2003).
[22] See EPAPS Document No. E-PRLTAO-103-006929 for supplementary material. For more information on EPAPS, see http://www.aip.org/pubservs/epaps.html.
[23] K. Hedberg *et al.*, Science **254**, 410 (1991).
[24] P. Hohenberg and W. Kohn, Phys. Rev. **136**, B864 (1964).
[25] W. Kohn and L. J. Sham, Phys. Rev. **140**, A1133 (1965).
[26] D. M. Ceperley and B. J. Alder, Phys. Rev. Lett. **45**, 566 (1980).
[27] J. P. Perdew and A. Zunger, Phys. Rev. B **23**, 5048 (1981).
[28] M. Stengel *et al.*, Phys. Rev. Lett. **91**, 166101 (2003).
[29] L.-L. Wang and H.-P. Cheng, Phys. Rev. B **69**, 045404 (2004).
[30] W. L. Yang *et al.*, Science **300**, 303 (2003).
[31] H. M. Polatoglou *et al.*, Phys. Rev. B **48**, 1877 (1993).
[32] A. J. Maxwell *et al.*, Phys. Rev. B **57**, 7312 (1998).
[33] R. Felici *et al.*, Nature Mater. **4**, 688 (2005).
[34] C. C. Kuo *et al.*, Surf. Rev. Lett. **14**, 739 (2007).
[35] M. Pedio *et al.*, Surf. Sci. **437**, 249 (1999).
[36] L. H. Tjeng *et al.*, Solid State Commun. **103**, 31 (1997).
[37] W. W. Pai *et al.*, Phys. Rev. B **69**, 125405 (2004).
[38] C. Tao *et al.*, Phys. Rev. B **73**, 125436 (2006).